



# HHS Public Access

Author manuscript

*Nat Neurosci.* Author manuscript; available in PMC 2016 August 01.

Published in final edited form as:

*Nat Neurosci.* 2016 February ; 19(2): 271–282. doi:10.1038/nn.4219.

## Activation of raphe nuclei triggers rapid and distinct effects on parallel olfactory bulb output channels

Vikrant Kapoor<sup>1,2,†</sup>, Allison Provost<sup>1,2</sup>, Prateek Agarwal<sup>1,2</sup>, and Venkatesh N. Murthy<sup>1,2,†</sup>

<sup>1</sup>Center for Brain Science, Harvard University, Cambridge, MA 02138

<sup>2</sup>Department of Molecular & Cellular Biology, Harvard University, Cambridge, MA 02138

### Abstract

The serotonergic raphe nuclei are involved in regulating brain states over time-scales of minutes and hours. We examined more rapid effects of serotonergic activation on two classes of principal neurons in the mouse olfactory bulb, mitral and tufted cells, which send olfactory information to distinct targets. Brief stimulation of the raphe nuclei led to excitation of tufted cells at rest and potentiation of their odor responses. While mitral cells at rest were also excited by raphe activation, their odor responses were bidirectionally modulated, leading to improved pattern separation of odors. *In vitro* whole-cell recordings revealed that specific optogenetic activation of raphe axons affected bulbar neurons through dual release of serotonin and glutamate. Therefore, the raphe nuclei, in addition to their role in neuromodulation of brain states, are also involved in fast, sub-second top-down modulation, similar to cortical feedback. This modulation can selectively and differentially sensitize or decorrelate distinct output channels.

### Introduction

Information processing in the brain is modulated by the state of the animal. Endogenous neuromodulators such as serotonin (5-hydroxytryptamine or 5-HT), acetylcholine and norepinephrine are differentially released in a state-dependent manner and alter the function of neural circuits by modifying the properties of neurons and synapses<sup>1,2</sup>. The serotonergic system is of particular interest because it has been linked to a wide variety of brain functions<sup>3–12</sup>. 5-HT is released by neuronal populations in raphe nuclei in the brainstem, which project throughout the brain<sup>11</sup> and activate a wide range of signaling pathways in a diverse array of neurons<sup>11,13</sup>.

Users may view, print, copy, and download text and data-mine the content in such documents, for the purposes of academic research, subject always to the full Conditions of use:[http://www.nature.com/authors/editorial\\_policies/license.html#terms](http://www.nature.com/authors/editorial_policies/license.html#terms)

<sup>†</sup>Corresponding authors: Vikrant Kapoor, 16 Divinity Ave, Cambridge, MA 02138, USA. [vk Kapoor@mcb.harvard.edu](mailto:vk Kapoor@mcb.harvard.edu), Venkatesh N. Murthy, 16 Divinity Ave, Cambridge, MA 02138, USA. [vmurthy@fas.harvard.edu](mailto:vmurthy@fas.harvard.edu).

Joint first authors

**Author Contributions** ACP, VK and VNM designed the project. ACP and VK performed *in vivo* experiments, ACP and PA performed and analyzed histological experiments, VK performed *in vitro* experiments. VK and ACP analyzed the data with VNM's guidance, VNM supervised the entire project. ACP, VK and VNM wrote the paper with input from PA.

**Competing Financial Interests** The authors declare no competing financial interests.

Although most studies on the serotonergic system have focused on the timescale of mood (hours to days), raphe neuron activity can also be modulated at sub-second time scales<sup>5,14,15</sup>, allowing it to have a dynamic impact upon ongoing behavior. Earlier studies have examined serotonergic modulation using exogenous application of agonists<sup>8,9,16,17</sup>. Recent advances in optogenetics allow the study of fast and direct effects of transmitter release from raphe axons, allowing spatial and temporal specificity. Importantly, one can also investigate the role of neurotransmitters other than 5-HT that are potentially released by raphe axons, particularly glutamate<sup>5,18,19</sup>

The serotonergic system is thought to modulate sensory processing<sup>8</sup>, including that in the olfactory system<sup>9,16</sup>, but the exact nature of such modulation remains unclear. The olfactory bulb (OB) receives odor information from the nose and is the first synaptic processing station in the olfactory system<sup>20</sup>. Incoming information is processed by several types of neurons and sent to multiple brain regions via the axons of mitral and tufted cells (MCs and TCs)<sup>20,21</sup>. TCs and MCs project to divergent downstream targets and carry distinct information<sup>20,22,23</sup>. The raphe nuclei send dense projections to the olfactory bulb (OB)<sup>24,25</sup> and can affect incoming information at the first synapse in the input layer<sup>9</sup>. *In vitro*, 5-HT can excite external tufted cells (ETCs)<sup>26</sup> and can elicit both inhibition and excitation in MCs<sup>27</sup>. How the raphe nuclei affect information leaving the OB under native conditions has remained unknown. Here we have used optogenetics, optophysiology, and electrophysiology to investigate how the activation of the raphe nuclei modulates the OB output at fast timescales *in vivo*. In particular, since the activity of neurons in raphe nuclei can fluctuate with behavior over sub-second time scales<sup>5,14,15,28</sup>, we set out to explore how brief increases in the activity of raphe neurons can alter early olfactory processing.

## Results

### Modulation of OB principal neurons at rest

We imaged, using multiphoton microscopy, the responses of MCs and TCs to brief activation of the raphe (Fig 1). MCs and TCs were labeled with calcium indicator GCaMP6s<sup>29</sup> in the Tbx21-Cre (T-box 21; also called Tbet) mouse line<sup>30</sup>, in which Cre recombinase is specifically and exclusively expressed in principal cells of the OB. The indicator was expressed by injection of AAV2.9 virus carrying flex GCaMP6s into the OBs of Tbx21-Cre mice (see Methods and Supplementary Fig. 1). Two to six weeks following virus injection, mice were anesthetized, and cranial windows were placed over the hindbrain (for implantation of a bipolar electrode in raphe, see Methods) and over the OBs (to image TCs and MCs). Placement of the stimulating electrode was validated with post-hoc histology (Fig. 1a). Most of our *in vivo* experiments were performed in anesthetized mice unless stated otherwise.

Since the raphe nuclei are known to be involved in the regulation of breathing<sup>31</sup>, we first examined whether the breathing rate was altered by brief stimulation of raphe. At the stimulation parameters used for the experiments in this study (three 1 ms pulses at 10Hz), no change in breathing rate was apparent (Fig. 1b, c). This indicates that modulation of MCs and TCs in our experiments was not caused by changes in breathing rate, which could alter how odors are sampled by mice and the dynamics of OB circuits<sup>32</sup>.

We identified TCs and MCs (Fig. 1d, g) based on the depth at which their somata were located and their morphology (see Methods, Supplementary Fig. 1). Brief stimulation of raphe evoked robust, repeatable excitation in single TCs from rest (Fig. 1e) and across a population of TCs (Fig. 1f). Although the excitation was large in many cells, other cells in the same region were not affected by raphe activation. The average fractional fluorescence increase was  $7.2 \pm 0.72\%$  (Fig. 1f; 288 cells from 12 animals, median change of 2.87 %), which was significantly different from zero ( $p = 9.80 \times 10^{-29}$ , Wilcoxon signed-rank).

We next examined the effects of raphe stimulation on MCs (Fig. 1g). Many, but not all MCs were excited by brief raphe activation (Fig. 1h). The average fractional fluorescence increase in MCs was  $5.1 \pm 0.91\%$  (Fig. 1i; 238 cells from 13 animals, median change of 2.24 %), which was significantly different from zero ( $p = 4.68 \times 10^{-10}$ , Wilcoxon signed-rank) and also significantly lower than that in TCs ( $p = 3.6 \times 10^{-5}$ , Wilcoxon rank-sum).

These results indicate that brief stimulation of raphe leads to fast excitation in both TCs and MCs at rest, which was surprising given the prior expectation of slow effects by neuromodulatory systems.

### Modulation of TC odor responses

Since raphe stimulation excited TCs at rest, we hypothesized that this excitation will affect odor responses. To test this hypothesis, we imaged odor-evoked responses in TCs (Fig. 2a and b) with and without raphe stimulation (three 1 ms pulses at 10Hz delivered one second into odor presentation). Two to 6 odors were chosen from a panel of 25 odors (Supplementary Fig. 2), based on a quick screen of responses for the collection of imaged cells in each experiment. Odors typically elicited fluorescence increases in TCs (Fig. 2b, c), which tended to be of larger amplitude when paired with raphe activation (Fig. 2b and c). Each cell's odor tuning profile was rank ordered based on the average odor response in the absence of raphe stimulation and then compared to the odor tuning profile with raphe activation (Fig 2d). Results from an exemplar experiment for 62 cells and 6 odors illustrate that there is an overall enhancement of odor responses with raphe stimulation (Fig. 2c and d). To quantify the effects of raphe modulation further, we calculated the number of odors to which individual cells responded under different experimental conditions. Within cell comparison indicated that TCs generally responded to a greater number of odors with raphe stimulation (Fig. 2e, mean change of  $2.4 \pm 0.06$  and median increase of 2 odors; significantly different from zero,  $p = 7.50 \times 10^{-13}$ , Wilcoxon signed-rank). These results indicate that the tuning widths of TCs, which are broad to begin with<sup>33,34</sup>, tend to be further broadened by raphe activation. The enhancement in odor responses (916 of 1087 cell-odor pairs showed significant increase, see Methods for details) and increase in the number of odors eliciting responses were robust (Fig. 2e) and consistent across experiments (bottom panels in Fig. 2e and f, mean change of  $2.9 \pm 0.04$  and median increase of 3 odors, 6 animals, significantly different from 0,  $p = 1.68 \times 10^{-10}$ , Wilcoxon signed-rank).

We observed significant diversity in the effects of raphe stimulation on the odor responses of TCs (Fig 2b, c and g). Odor responses were differentially modulated in different TCs, (Fig. 2b,c,g), and even in the same cell, raphe stimulation had distinct effects on responses to different odors (Fig. 2b, c and d; Supplementary Fig. 3). We next asked what might predict

the TC odor responses in presence of raphe stimulation by performing four different types of regression analysis on the data (see Methods for details). Neither raphe responses nor odor responses in isolation predicted TC responses to concurrent odor and raphe stimulation ( $R^2 = 0.10$  and  $R^2 = 0.66$  respectively for raphe and odor stimulation, Fig. 2g), but a linear regression model utilizing both raphe and odor responses as variables performed much better ( $R^2 = 0.79$ ). Importantly, a regression model that also included a term for interaction between the raphe and odor responses (interactive regression model) performed the best ( $R^2 = 0.88$ , Fig. 2h). The four parameter fit was better than the three parameter fit according to standard goodness of fit measures ( $p = 1.29 \times 10^{-21}$ , F test, Supplementary Fig. 3). We also found that this predictive model was consistent across different odors (Fig. 2i), as well across multiple animals (Fig. 2j).

Previous experiments indicated that strong electrical stimulation of the raphe reduced odor-evoked responses in olfactory sensory axons (OSNs)<sup>9</sup>. Using a mouse line in which GCaMP3 is expressed exclusively in OSNs, and found that brief stimulation of the raphe (three 1ms pulses at 10 Hz) does not alter odor-evoked responses in the sensory inputs (Supplementary Fig. 4).

These data suggest that raphe inputs to the OB provide a means of sensitizing TCs, increasing the probability of TCs responding to odors and also enhancing existing odor responses of TCs.

### Modulation of MC odor responses

We next explored how MC odor responses are modulated by raphe activation using GCaMP6s to image their odor-evoked responses (Fig. 3a, and b). Surprisingly, MC odor responses could be both suppressed and enhanced by raphe activation (Fig. 3b, c, 770 of 1050 cell odor pairs showed significant modulation, see Methods for details). The double rank ordered plots indicate that some odor responses increased while others decreased, and that this is not stereotyped within a cell (Fig. 3d) or within an odor. Interestingly, pairwise comparison of individual MCs with and without raphe activation indicated a broad range of changes including both increase and decrease in the number of odors that evoke responses (Fig. 3e, top), but with no systematic change across the population (Fig. 3e, mean change in the number of odors was  $0.1 \pm 0.08$  and median change of 0, not significantly different from 0,  $p = 0.61$  for  $n=47$  cells for Wilcoxon signed-rank) and these results were consistent across animals (Fig. 3e, mean change in the number of odors was  $0.0 \pm 0.04$ , median change of 0, not significantly different from 0,  $p = 0.85$  for 1050 cells from 7 animals, Wilcoxon signed-rank). In contrast to TCs, (Fig. 2e and f), the number of odors that activated a given MC was the same, on average, with and without raphe activation (Fig. 3e) and there was no systematic increase in the responses of MCs (Fig. 3f,  $p = 0.9$  for 1050 cells from 7 animals for Wilcoxon signed-rank). The bidirectional nature of MC modulation is, therefore, distinct from TC modulation.

The modulation of MCs showed remarkable diversity (Fig. 3 g), dependent upon the cell identity as well as odor identity. We asked whether the regression analysis we performed for TCs would also be able to predict MC enhancement/suppression. We found that even the

interactive model was poor at predicting the modulation of MC odor responses in presence of raphe stimulation (Fig. 3h).

These data indicate that MC odor responses are bidirectionally modulated by brief raphe activation, and this modulation is dissimilar to that measured in TCs.

### Selective stimulation of raphe axons

The effects reported above involved electrical stimulation of the raphe nucleus. To confirm that these effects were due to specific excitation of the raphe nuclei, we turned to a transgenic mouse line (TPH2-ChR2-YFP) in which channelrhodopsin-2 (ChR2) is expressed specifically in serotonergic neurons<sup>35</sup>. These neurons and axons can be selectively activated using light stimulation in the raphe or the OB. We confirmed that raphe projections are found throughout the different layers of the OB using the fluorescence of YFP, which is coexpressed with ChR2 (Fig. 4a and Supplementary Fig. 5).

We recorded from single putative MCs or TCs (M/TCs) on the dorsal surface of the OB using tungsten electrodes and stimulated raphe axons with blue light (three 10 ms pulses at 10 Hz, 15 mW/mm<sup>2</sup> of power). Brief and specific activation of raphe fibers increased the firing rates in the recorded units (Fig. 4b and c; n = 17 units). This excitation was not due to nonspecific effects such as light-induced heating since none of the 8 cells recorded from wild-type animals were significantly modulated (data not shown).

To compare the optical and electrical stimulation more directly, we recorded from M/TCs as described above and additionally inserted a bipolar stimulating electrode into raphe nucleus. Fast excitation was elicited by both optogenetic activation and electrical stimulation (Fig. 4d, left), although the time courses differed. Importantly, 3 of the 9 cells that were significantly modulated by electrical activation of raphe were also significantly modulated by optogenetic stimulation (Fig. 4d, right). On average, the firing rate increased 20-fold ( $\pm 12$ ) and 40-fold ( $\pm 28$ ) from baseline, with optogenetic stimulation and electrical stimulation, respectively.

To further characterize the effects of optical stimulation of the raphe on OB principal neurons, we labeled neurons in the OB with GCaMP6s using a non-conditional AAV2.9 virus injected in TPH2-ChR2 mice (see methods for details). This strategy led to labeling of many cell types in the OB, with lower numbers of labeled TCs and MCs than when using the flex virus in Tbx21-Cre animals, but these principal cells could be readily identified based on their morphology and depth. To stimulate raphe neurons optically, we implanted an optical fiber (see Methods for details) in the raphe nucleus of these animals. We imaged the activity of both MCs and TCs during optogenetic activation of raphe, with and without odor stimulation (Fig. 4e and h). Similar to our results for electrical stimulation (Fig. 2c), we found that the TC odor responses were potentiated by brief raphe activation (Fig. 4e, f and g, 96 of 144 cell-odor pairs from 3 animals showed significant potentiation) with a mean change of  $27.53 \pm 2.3$  % ( $p = 1.2 \times 10^{-23}$  for Wilcoxon signed-rank test, median change of 20.82 %), whereas the modulation in MC odor responses was bidirectional (41 of 64 cell odor pairs from 2 animals showed significant modulation, Fig. 4 h, i and j, mean  $1.69 \pm 3.9$  % and median change of 1.29 %, see Methods).

These data suggest that the distinct modulatory effects on the two principal neuronal populations of the OB are due to specific activation of serotonergic neurons in the raphe.

### Activation of raphe axons modulates TC activity in vitro

The distinct and differential modulation of TC and MC network prompted us to explore the cellular and synaptic mechanisms underlying these effects using acute OB slices and whole cell patch clamp recordings<sup>36</sup>. We first measured synaptic responses of TCs to raphe inputs in slices from the TPH2-ChR2-YFP mouse. A patch pipette was targeted to TCs in the external plexiform layer (Fig. 5a), and excitatory and inhibitory currents were recorded under voltage clamp at  $-70\text{mV}$  and  $0\text{mV}$ , respectively.

Blue light stimulation (three 10ms pulses at 10 Hz) elicited both inhibitory and excitatory currents in TCs (Fig. 5b). Excitatory and inhibitory currents were asynchronous and lasted for hundreds of milliseconds (Fig. 5b, right). We quantified both excitatory and inhibitory events by calculating the total charge transferred at  $-70\text{mV}$  and  $0\text{mV}$  (Fig. 5c, d). Excitatory events were initiated quickly and inhibitory events were delayed, as judged by the time points at which the light-stimulated traces diverge from control traces (Fig. 5c). Targeted raphe fiber stimulation increased excitatory charge by  $0.0287 \pm 0.003\text{ nC}$  (median change of  $0.0277\text{ nC}$  and  $p = 3.1 \times 10^{-27}$  for 6 cells from 4 animals, Wilcoxon signed-rank test) and inhibitory charge by  $0.41 \pm 0.08\text{ nC}$  (median change of  $0.4128\text{ nC}$  and  $p = 3.3 \times 10^{-3}$  for Wilcoxon signed-rank test,  $n = 6$  cells).

We used pharmacological manipulations to uncover the molecular basis of light-evoked responses in TCs. Surprisingly, methysergide ( $50\text{ }\mu\text{M}$ ), a broad-spectrum 5-HT receptor antagonist, led to increased excitation onto TCs ( $143.82 \pm 2.52\%$  of the no drug control,  $p = 5.01 \times 10^{-4}$ , Wilcoxon rank-sum test,  $n = 8$  cells; Fig. 5e, left), rather than blocking the effect. Methysergide also reduced light-evoked inhibitory currents measured at  $0\text{mV}$  ( $70.83 \pm 14.76\%$  of no drug control,  $p = 3.92 \times 10^{-3}$ , Wilcoxon rank-sum test,  $n = 8$  cells; Fig. 5e, right). By contrast, raphe excitation onto TCs was blocked by ionotropic glutamate receptor blockers ( $50\text{ }\mu\text{M}$  AP5 and  $20\text{ }\mu\text{M}$  CNQX,  $p = 7.61 \times 10^{-29}$ , Wilcoxon rank-sum test,  $n = 7$  cells, Fig. 5e) and part of the inhibition was also blocked by these drugs ( $39.10 \pm 5.31\%$  of no drug control,  $p = 2.10 \times 10^{-7}$ , Wilcoxon rank-sum test,  $n = 7$  cells, Fig. 5e). Together, these results suggest that both glutamate and 5-HT release contribute to the modulation of electrical activity in TCs. TC excitation was increased by application of GABA<sub>A</sub> receptor blocker,  $20\text{ }\mu\text{M}$  gabazine ( $128.74 \pm 9.68\%$  of no drug control,  $p = 2.0 \times 10^{-3}$ , Wilcoxon rank-sum test,  $n = 6$  cells)(Fig. 5e), and inhibition was blocked ( $2.58 \pm 1.30\%$  of no drug control,  $p = 1.92 \times 10^{-21}$ , Wilcoxon rank-sum test,  $n = 6$  cells, Fig. 5e).

To explore the effect of raphe axon activation on the spiking activity of TCs, we recorded from TCs in current clamp mode (Fig. 5f), and promoted spike firing by injecting different amount of currents, while probing with blue light 500 ms after the onset of current step. TC firing rates were potentiated by light stimulation across all current injections (Fig. 5g and h;  $50.15 \pm 8.95\%$ ,  $p = 1.21 \times 10^{-3}$ , Wilcoxon rank-sum test,  $n = 5$  cells), mimicking the potentiation in odor responses recorded *in vivo* (Fig. 2b). Potentiation of TC firing rate was blocked by ionotropic glutamate receptor blockers ( $50\text{ }\mu\text{M}$  AP5 and  $20\text{ }\mu\text{M}$  CNQX,  $p = 1.43 \times 10^{-8}$ , Wilcoxon rank-sum test,  $n = 5$  cells; Fig. 5g, h), which also uncovered an



inhibitory modulation by raphe axons (Fig. 5g, h;  $-8.01 \pm 4\%$  in presence of AP5 and CNQX compared to no drug control,  $p = 1.43 \times 10^{-8}$ , Wilcoxon rank-sum test,  $n=5$  cells). Interestingly, blocking 5-HT receptors ( $116.15 \pm 15\%$  of no drug control,  $p = 0.072$ ,  $n=5$  cells) or GABA<sub>A</sub> receptors ( $133.60 \pm 14.10\%$  of no drug control,  $p = 0.068$ ,  $n=5$  cells; Fig. 5g, h) increased the degree of potentiation. Firing rates also increased for TCs at rest ( $4.38 \pm 0.48$  Hz,  $p = 9.21 \times 10^{-3}$ , Wilcoxon rank-sum test,  $n = 5$  cells, see arrow in Fig. 5g and also shown in Fig. 5f), similar to the effect of raphe stimulation on basal fluorescence of TCs *in vivo* (Fig. 1d–f). This excitation was blocked by AP5 & CNQX ( $p = 1.44 \times 10^{-6}$  for Wilcoxon rank-sum test,  $n = 5$  cells, Fig 5h), but was increased by both methysergide and gabazine ( $168.91 \pm 56.21\%$  and  $173.45 \pm 43.81\%$  compared to no drug control, respectively;  $p = 2.74 \times 10^{-4}$  and  $1.90 \times 10^{-5}$  respectively, Wilcoxon rank-sum test,  $n = 5$  cells) (Fig. 5h).

Together, these data indicate that optogenetic activation of raphe axons elicited large excitatory currents in TCs both at rest and when they were active. In addition to this excitation primarily driven by glutamate, there was an inhibitory component driven through 5-HT receptors and local GABAergic circuits in the OB.

### Activation of raphe axons modulates MC activity *in vitro*

We next asked how raphe modulation of MC firing compares with that of TCs by recording from MCs *in vitro* (Fig. 6a, b). Comparable to our *in vivo* results (Fig. 1g–i), MCs were activated from rest (Fig. 6c, see arrow, increase of  $10.01 \pm 3.32$  Hz,  $p = 2.0 \times 10^{-3}$ , Wilcoxon rank-sum test,  $n = 7$  cells from 4 animals), but were bi-directionally modulated by light when they were induced to fire spikes through current injection (Fig. 6b, c). This effect contrasts with that on TCs, which were uniformly potentiated by light stimulation of raphe axons (Fig. 5g). Interestingly, individual MCs could be either potentiated or inhibited, and there was no systematic dependence on firing rate (Fig. 6b). Furthermore, we found that the excitation to inhibition ratio (see Methods for details) for MCs varied significantly more (Fig. 6d, e) than that of TCs (mean 0.08 and 0.11 and standard deviation 0.065 and 0.092 for TCs and MCs respectively).

Application of methysergide largely blocked the inhibitory MC modulation (Fig. 6f), resulting in an overall potentiation of firing rate ( $201.58 \pm 9.20\%$  of the no drug condition,  $p = 1.1 \times 10^{-19}$ , Wilcoxon rank-sum test,  $n = 5$  cells from 3 animals; Fig. 6g). Conversely, application of AP5 and CNQX blocked the excitatory effect (Fig. 6f), with a net reduction of firing rate ( $-29.88 \pm 15.42\%$  of no drug condition,  $p = 7.2 \times 10^{-31}$ , Wilcoxon rank-sum test,  $n = 5$  cells, Fig. 6g). This indicates that, similar to what we measured in TCs, 5-HT had an inhibitory effect, while glutamate was responsible for the excitatory effect. In fact, 5-HT appears to have a greater inhibitory effect in MCs (Fig. 6g) than TCs (Fig. 5h, right). Some of the inhibitory effects were also mediated by GABA<sub>A</sub> receptors since gabazine increased the firing rates ( $147.14 \pm 11.38\%$  of no drug control,  $p = 8.79 \times 10^{-3}$ , Wilcoxon rank-sum test,  $n=5$  cells; Fig. 6f, g). MC recordings *in vitro* strongly corroborated the effects on MC odor responses observed *in vivo* (Fig. 3b and c), with single MCs *in vitro* exhibiting both excitation and inhibition of their firing rates. Whether modulation was excitatory or inhibitory was dependent on firing rate for each MC, but the crossover point, where modulation shifted from inhibition to excitation or vice versa, varied from cell to cell (Fig.

6b). This complexity and lack of predictability of MC modulation may be attributable to network effects and the increased lateral inhibition on MCs as compared to TCs, and perhaps also the cell to cell variability in 5-HT receptor expression (see Supplementary Fig. 1).

In summary, unlike TCs whose firing rates are potentiated by raphe inputs, MC firing rates were bi-directionally modulated, similar to what was documented *in vivo*.

### External tufted cells receive fast inputs from raphe axons

Although MCs and TCs both exhibited fast effects from raphe axon activation, the timing of the light-evoked currents strongly suggested polysynaptic pathways for these effects (Fig. 5b, and 6d). Therefore, we sought to identify the cell type in the OB that receives direct synaptic inputs from raphe terminals and could account for the excitatory effects recorded in MCs and TCs. We hypothesized that these recipients could be external tufted cells (ETCs), which reside at the base of the glomerular layer and possess a single dendrite that projects into a nearby glomerulus (Fig. 7a). ETCs receive direct inputs from OSNs, and release glutamate to excite MCs and TCs at the same glomerulus<sup>37,38</sup>. Moreover, ETCs express 5-HT receptors and have been shown to be sensitive to pharmacological application of 5-HT<sup>26,27</sup>. In addition, the glomerular layer has denser innervation of raphe axons (Supplementary Fig. 5) as compared to other layers in the olfactory bulb<sup>24</sup>.

Whole cell recordings from ETCs (Fig. 7a) revealed light-activated excitatory postsynaptic currents (EPSCs) aligned closely with each light pulse (Fig. 7b,c; see Methods). Light-evoked EPSCs were blocked by AP5 and CNQX (data not shown) indicating that they are glutamatergic. These EPSCs were reliable (8% failure rate) and had an average latency of  $4.39 \pm 0.39$  ms (median latency of 3.1 ms) after the onset of blue light (Fig. 7b, d). This timing is congruent with monosynaptic input from raphe axons onto ETCs, similar to that of OSNs<sup>37,38</sup>. By contrast, the latencies of responses in TCs ( $14.49 \pm 0.49$  ms and median of 13.3 ms,  $p = 3.2 \times 10^{-17}$  for 5 animals, Wilcoxon rank-sum) and MCs ( $15.26 \pm 0.53$  ms and median of 13.6 ms) were substantially longer ( $p = 2.4 \times 10^{-20}$  for 3 animals, Wilcoxon rank-sum test, Fig. 7b, d).

These data suggest that ETCs receive direct excitatory, glutamatergic input from raphe axons, and they, in turn, activate glomerular networks, leading to the excitatory and inhibitory currents observed in TCs and MCs.

### Raphe inputs differentially affect MC and TC coding

The OB is the first station in the brain for olfactory processing, and ensembles of MCs and TCs send potentially different odor information from the OB to different regions of the brain<sup>20,23</sup>. Given that both TCs and MCs are strongly modulated by brief activation of raphe projections, we next explored how the raphe mediated modulation of odor responses influences the coding strategies of these cells.

One potential way to enhance the discriminability of different odors by the downstream circuit is to increase the linear separability of patterns of activity of the bulbar output neurons<sup>39</sup>. To elucidate the changes in separability, we performed an unbiased analysis of





responses that matched those produced by electrical stimulation of the raphe. Fourth, the results of our *in vivo* experiments matched the *in vitro* experiments (where specific optical stimulation was used exclusively)– TC activity was always potentiated but MC activity was modulated in a bidirectional manner. These arguments strongly support the specificity of raphe stimulation.

All the data presented above were from anesthetized animals, which afforded better control, reduced variability and minimized contributions from other neuromodulatory systems. We acknowledge, however, that anesthesia alters many aspects of neuronal and synaptic function, as well as the baseline activity of raphe neurons<sup>11</sup>. Although extensive future studies in awake behaving animals are necessary to compare raphe modulation of OB function in different behavioral states, our preliminary experiments in awake mice have confirmed the key results on TC and MC modulation by raphe stimulation (Supplementary Fig. 6).

### Rapid effects mediated by glutamate

Serotonergic signaling is important on timescales that vary from seconds to hours. It is implicated in the evaluation of punishment and reward on short time scales<sup>4,5,14</sup>, control of breathing and body temperature on the time course of minutes<sup>31</sup>, and modulating mood and brain states on longer time scales<sup>3,4</sup>. Interestingly, brief activation of raphe neurons can drive reward behavior<sup>5</sup>, and this fast reward signal appears to be primarily glutamatergic. Slightly longer duration activation can promote patience in subjects<sup>7,40</sup>. Our current results indicate that brief activation of raphe neurons has robust and diverse effects on early olfactory processing.

Activation of raphe axons leads to excitation in principal neurons in the OB, as well as delayed inhibition. Excitation in ETCs occurred at short latencies and was abolished by ionotropic glutamate receptor blockers, suggesting direct release of glutamate from raphe terminals. By contrast, most of the excitation seen in TCs and MCs was delayed and asynchronous, indicative of recurrent excitation within the OB. Previous studies have shown that ETCs excite TCs and MCs through dendritic release of glutamate<sup>37,38</sup>, offering a plausible mechanism of polysynaptic excitation. 5-HT positive axons have been shown to synapse onto both GABAergic and non-GABAergic targets in the glomerular layer<sup>41</sup>. Inhibitory currents activated by raphe stimulation were also polysynaptic, since they were blocked by glutamatergic blockers. Depolarization of ETCs, and subsequently TCs and MCs, will likely recruit glomerular layer interneurons and granule cells<sup>20</sup>, which can induce GABAergic currents in principal cells. Whether interneurons are directly excited by raphe axons must await future experiments. The net result of the dual effects on the firing rates of TCs and MCs was complex and is discussed below.

### Dual release of 5-HT and glutamate by raphe axons

A key inference from our findings is the dual release of glutamate and 5-HT from raphe terminals. We found evidence for release of 5-HT with brief activation: in both TCs and MCs, methysergide led to a reduction in light-activated inhibition suggesting that 5-HT had a net inhibitory action on principal neurons. Whether this action is due to direct inhibition

through 5-HT<sub>1</sub> receptors on principal neurons (Supplementary Fig. 1) or through excitation of 5-HT<sub>2</sub> receptors on interneurons<sup>26,27</sup>, remains to be studied. Since the effects of raphe axon stimulation were more strongly modulated by glutamatergic blockers, we predict that only modest release of 5-HT is triggered by our brief stimulation.

Previous studies have shown that many of the 5-HT producing neurons of the raphe also express VGluT3, a vesicular glutamate transporter<sup>5,42–44</sup>, which have been detected ultrastructurally in identified serotonergic axons<sup>18</sup>. Glutamate release from raphe fibers was shown to play a significant role in raphe modulation of behavior<sup>5,44</sup> and hippocampal activity<sup>19</sup>. In our experiments, optogenetic activation of identified raphe axon terminals in the OB had modulatory effects due to both 5-HT and glutamate, but whether these neurotransmitters are released from the same or distinct synaptic sites, and whether the relative amount of 5-HT and glutamate release is activity dependent<sup>5</sup> remains unclear.

This interplay between glutamate release and 5-HT release could bridge the gap between sensing/behavior and mood/state of being. Recent studies have shown that 5-HT modulates the OB or the analogous insect circuit at multiple sites<sup>9,16,26,27</sup>. Previously our lab showed that 5-HT activates inhibitory periglomerular cells in the glomerular layer of the OB that then inhibit incoming olfactory sensory axons, resulting in presynaptic inhibition<sup>9</sup>. In these earlier experiments, the raphe was activated for many minutes and 5-HT receptor antagonists blocked the effect, whereas in the experiments described here brief raphe stimulation did not alter glomerular input (Supplementary Fig. 4). These differences indicate that the modulatory effects of raphe projections are dependent on the time scale and degree of activity. Notably, the rapid effects of raphe activation on TCs and MCs are similar to the actions of cortical feedback to the OB<sup>45</sup>, blurring the distinction between neuromodulation and ongoing computation.

### Differential modulation of TCs and MCs

An exciting and unexpected finding from our experiments is that MCs and TCs are differentially modulated by brief activation of raphe inputs. MCs and TCs are the two main types of principal neurons in the OB, and they differ both anatomically and functionally. Their somata reside in different layers of the olfactory bulb circuit<sup>20</sup>, and their downstream targets also diverge<sup>20,21,23</sup>. TCs send axons to more anterior targets, while MCs project to both anterior and posterior olfactory cortical areas<sup>20</sup>. Functionally, TCs are intrinsically more excitable<sup>46</sup> and respond to a wider range of odors and concentrations than MCs<sup>33,34,47</sup>.

Our experiments show that these two subtypes of cells also differ in the way they are modulated by raphe inputs. We have focused on time-averaged activity in this study, leaving open potential differences in the raphe effects on temporal dynamics of TC and MC activity. It is clear that neuromodulators play an important role in olfactory processing<sup>9,48–50</sup>, but our study is the first to show that neuromodulators can differentially affect MCs and TCs. MCs tend to be more decorrelated than TCs, and brief raphe inputs drove these two subtypes even farther apart—TC odor responses became more correlated while MC odor responses were further decorrelated. Although both cell types received light-triggered excitation as well as inhibition, the overall effect on TCs was invariably excitatory. This could be because excitation arrives earlier in TCs and inhibition is weaker and rarely occurs without earlier

excitation. One possible circuit mechanism for this effect might be weaker lateral inhibition on TCs, with most inhibition arising from the intraglomerular circuits. By contrast, each MC appeared to receive a distinct balance of excitation and inhibition, such that the net effect of firing can be in either direction. Perhaps MC inhibition can also occur without much excitation due to more robust interglomerular lateral connections.. Interestingly, different raphe nuclei may preferentially target distinct layers of the OB<sup>25</sup>, offering another potential source of differential effects on OB neurons.

This differential modulation of TCs and MCs may be behaviorally relevant for animals to both detect and identify stimuli. The sensitization of TCs may lead to more efficient detection of behaviorally relevant stimuli in anterior olfactory cortex, while the decorrelation of MC representation could lead to increased accuracy in identification of odors in more distal cortical areas. The synergy of these two modulatory effects could lead to improved encoding of the olfactory world.

## Methods

### In vivo imaging experiments

All procedures were performed using approved protocols in accordance with institutional (Harvard University Institutional Animal Care and Use Committee) and national guidelines. For *in vivo* 2-photon imaging experiments, Tbx21-Cre mice were used<sup>30</sup>. Mice (age 2–6 months) were anesthetized with a mixture of ketamine (100mg/kg) and xylazine (10mg/kg) and placed in a stereotaxic apparatus (in accordance with Harvard University animal welfare guidelines). A small craniotomy was performed over each olfactory bulb (OB) and 200 nL of AAV2.9 virus (UPenn Vector Core) carrying flex GCaMP6s<sup>51</sup> was injected 1mm deep in each OB through a glass micropipette attached to a nanoinjector (MO-10, Narishige).

Three to six weeks after injection, mice were anesthetized and a custom-built titanium head plate was secured to their skull with bone cement (Dentsply). A cranial window was placed 3.5 mm lateral to lambda. A bipolar electrode (FHC) was stereotaxically placed in the raphe at a 45 degree angle, –4.25mm posterior of bregma, 0 medial-lateral, 3.5 mm deep. A second cranial window was placed over the OBs to expose their dorsal surface. 1.2% agarose in saline and a coverslip were placed over the second cranial window for imaging. Sterile saline was used as the fluid for the immersion objective.

For optogenetic experiments, TPH2-ChR2-YFP<sup>35</sup> mice were injected with non-conditional AAV GCaMP6s virus. Two to four weeks after injection, an optical fiber (300 μm core, Polymicro technology) was implanted in the raphe, and the fiber was coupled to a 473 nm blue DPSS laser (LASERGLow Technology). The laser was shuttered using a custom-built shutter to allow timed stimulation.

For awake experiments, a custom-built bipolar electrode (0.0002” coated SS wire, A-M systems) was implanted in the raphe and attached to the skull via magnets (0.0625” disc magnets, MAGCRAFT).

Breathing was monitored via a stress sensor (Kent Scientific) placed around the abdomen. A custom-built microscope was used for *in vivo* imaging as described previously<sup>9</sup>. Calcium indicators were excited and imaged (4–20 Hz) with a water immersion objective (20x, 0.95 NA, Olympus) at 927 nm using a Ti:sapphire laser (Chameleon Ultra, Coherent) with a 140-fs pulse width and 80-MHz repetition rate. Image acquisition, scanning, and stimulus delivery were controlled by custom-written software in LabVIEW (National Instruments). Odors were delivered via a custom-built olfactometer as described previously<sup>52</sup>. For odor trials, odors were delivered for 3 seconds after 5-10s of baseline. Each odor presentation was repeated at least 2 times for both odor-only and odor-plus-raphé stimulation trials. Stimulation and non-stimulation trials were interleaved, and blank trials in which no odor or stimulation (clean air only) were given were also interspersed. Odors were diluted in diethyl phthalate solvent (Sigma-Aldrich) at 5% v/v (Supplementary Fig. 2 has the list of odors used). Electrical stimulation (250  $\mu$ A, three 1 ms biphasic pulses at 10Hz; negative peak first; SD9 Grass) of the raphe began one second after odor onset. Electrical stimulation signals were recorded for each stimulation trial to ensure timing and current amplitude. In baseline excitation trials, stimulation was initiated 5-10s after trial onset. As with the odor trials, non-stimulation and stimulation trials were interleaved, with stimulation trials repeated at least 3 times.

At the termination of the experiment, an electrolytic lesion was made in order to check the position of the bipolar electrode in the raphe (10 seconds, square pulse, 5 mA). Mice were transcardially perfused, and the brains were removed from the skull. Coronal floating sections were cut using a vibratome (Leica VT1000S). Only mice with a clear lesion ventral to the central aqueduct were included in the data analysis. Although the electrolytic lesion was clear in the floating sections, some sections were mounted and Nissl staining performed. Sections were dried overnight, followed by staining with filtered cresyl violet blue solution (500 ml distilled water, 2.5g cresyl violet acetate, 1.5ml glacial acetic acid), and then dehydrated using a series of ethanol dilutions (50%, 60%, 80%, 90%, 95%, and 100%), cleared with xylenes, and cover-slipped using Cytoseal 60. Slides were imaged using a Zeiss AxioImager Z2.

### Identification of cells

For *in vivo* imaging experiments, we used Tbx21-Cre animal, where cre recombinase is selectively expressed in the principal neurons (MCs, TCs and ETCs) of the OB<sup>30</sup> (Supplementary Fig. 1 and Supplementary Movie 1). We used depth and the cell body location within a specific layer (MCL or EPL) as a criterion to classify the cell identity. As shown in Supplementary Fig. 1 and Supplementary Movie 1, our viral injection resulted in sparse labeling of cells in EPL and MCL; cells located in the EPL were classified as TCs and the cells in the MCL were classified as MCs.

For *in vitro* slice electrophysiology experiments, we used previously well-established criteria to classify the cells. Principal neurons of the OB have significantly larger cell bodies compared to the inhibitory neuronal populations in the OB. Similar to previous studies, cells with >50% of the cell body lying in MCL were classified as MCs. Neurons that were entirely situated in the EPL were classified as TCs. To identify and record from ETCs, we

perform cell attached recordings from the cells with large cell bodies close to the glomerular layer and the cells that showed rhythmic bursting were used for whole cell patch recordings.

### In vivo electrophysiology

For *in vivo* electrophysiology, transgenic TPH2-ChR2-YFP mice were used<sup>35</sup>. For ChR2 negative controls, we used C57/B6 mice (Jax.org). Mice (age 2–8 months) were anesthetized, as mentioned above, with a mixture of ketamine (100mg/kg) and xylazine (10mg/kg) and fitted with a head plate that was secured with bone cement (Dentsply). A single cranial window was placed over one OB. MC and TC signals were recorded using tungsten electrodes (1–5 M $\Omega$ ; FHC). Signals were amplified and filtered (100 Hz – 1 MHz) and sampled at 20 kHz (A-M Systems). ChR2 was activated by three 10 ms blue light pulses shone on the surface of the cranial window at 10Hz (~15 mW/mm<sup>2</sup>). Trials were spaced by at least 15 seconds, and light trials were repeated 10–50 times.

Spikes with amplitudes greater than 5 times the standard deviation of the baseline were sorted manually according to their projections into principal component space. We only accepted cells with at least 95% of spikes exhibiting an interspike interval greater than 3 ms. Significance of PSTHs was determined by comparing the average rate during a 5-second period following blue light activation with a corresponding period with no light using a sign test.

### In vitro electrophysiology

Slices were prepared using methods adapted from previous work<sup>36</sup>. Mice (4–12 weeks old, TpH2-ChR2-YFP) were deeply anesthetized with a mixture of ketamine (100mg/kg) and xylazine (10mg/kg) and then perfused with ice-cold modified ACSF solution (in mM: 120 choline chloride, 25 glucose, 25 NaHCO<sub>3</sub>, 2.5 KCl, 0.5 CaCl<sub>2</sub>, 10 MgSO<sub>4</sub>, 5 sodium ascorbate, 3 sodium pyruvate, 1.25 NaH<sub>2</sub>PO<sub>4</sub>.H<sub>2</sub>O). Brains were removed and placed in the same ice-cold modified ACSF. Sagittal slices (300  $\mu$ m thick) of olfactory bulbs were cut using a vibratome (VT1000S; Leica, Germany). After cutting, slices were incubated in the above-mentioned ACSF solution (continuously oxygenated) at 37°C for 30 min before being transferred to oxygenated ACSF (in mM: 25 NaCl, 2.5 KCl, 25 NaHCO<sub>3</sub>, 1.25 NaH<sub>2</sub>PO<sub>4</sub>.H<sub>2</sub>O, 1 MgSO<sub>4</sub>, 25 glucose, 2.0 CaCl<sub>2</sub>).

Whole-cell current clamp recordings were made using patch pipettes filled with internal buffer (in mM: 120 potassium gluconate, 2.0 sodium gluconate 10 HEPES, 4.0 Mg ATP, 2.0 Na<sub>2</sub>ATP, 0.3 Na<sub>3</sub>GTP, 4.0 NaCl, and, 1% biocytin) and voltage clamp recordings were made using internal buffer (in mM: 130 D-Gluconic acid, 130 cesium hydroxide, 5.0 NaCl, 10 HEPES, 12 di-tris-P-creatine, 1 EGTA, 3.0 MgATP, 0.2 Na<sub>3</sub>GTP with 1% biocytin) using a Multiclamp 700B amplifier (Molecular Devices, Palo Alto, CA). Cells were visualized under custom build infrared optics on a BX51WI microscope (Olympus Optical, Tokyo, Japan). Physiological data were collected via software written in LabVIEW (National Instruments) and pClamp 10.3 (Molecular Devices). All recordings were performed at 35 °C in regular oxygenated ACSF unless mentioned otherwise. Pharmacological agents, gabazine (SR 95531 hydrobromide), DL-AP5, CNQX and methysergide maleate (all from Tocris Bioscience), were added as indicated in the main text.



We used a bright light-emitting diode (LED) array (CBT-90B, Luminus Devices) with peak emission at 465nm that was coupled to the rear lamp-housing of an Olympus BX51 upright microscope, with an intensity of 6–12 mW/mm<sup>2</sup> in the plane of the slice<sup>53</sup>. Three brief pulses of blue light of 10 ms each at 10 Hz were used to activate the ChR2 positive axon fibers. Trials were spaced by at least 60 seconds and stimulated (blue light) and unstimulated trials were interspersed.

To characterize the effect of light stimulation, we calculated the charge transferred as the area under the curve for the entire duration ~ 1.3 seconds of the recording under voltage clamp (both for 0 mV and –70 mV recordings). In order to calculate the E/I (excitatory to inhibitory charge) ratio, we calculated the absolute change in the charge transfer for both conditions ~ 0 mV and –70 mV and divided them to get the unit-less number.

## Data Analysis

**Image analysis**—Data were analyzed with custom software (Matlab). The different frames of a given stack were first registered using a cross-correlation-based registration algorithm (dftregistration.m in Matlab). Raw fluorescence time course was calculated from each region of interest. Fluorescence changes were expressed as a fraction of the baseline fluorescence, or  $\Delta F/F_0$ , where  $F_0$  was the average fluorescence over the 5 seconds preceding odor onset or raphe stimulation onset, in odor and baseline trials, respectively. Average integrated odor responses were calculated over a 7 second window starting at odor onset for odor trials and stimulation onset for baseline activation trials. To determine the number of odors to which single neurons responded, we used a threshold value of 3.0x the standard deviation of the same 7 seconds from blank (no odor, no stimulation) trials and the same criterion was also used to determine the number of cells that showed significant modulation in their responses

**Regression analysis**—We performed the following single variable or mutli-variable regression analysis for predicting neuronal responses to the combined effect of odor and raphe stimuli.

Single variable linear regression:

$$y = \beta_1 + \beta_2 x_1$$

where,

y is the predicted response of a given neuron to odor delivery in presence of raphe activation.

$x_1$  is the response of the same neuron to either odor input or raphe stimulation.

$\beta_1$  is a constant and

$\beta_2$  is the weight for the odor or raphe stimulation.

Multi variable linear regression:

$$y = \beta_1 + \beta_2 x_1 + \beta_3 x_2$$

where,

$y$  is the predicted response of a given neuron to odor delivery in presence of raphe activation.

$x_1$  is the response of the same neuron to odor stimulus.

$x_2$  is the response of the same neuron to raphe stimulation.

$\beta_1$  is a constant term and

$\beta_2$  and  $\beta_3$  are weights for the odor and raphe stimulations respectively.

Interactive regression model:

$$y = \beta_1 + \beta_2 x_1 + \beta_3 x_2 + \beta_4 x_1 x_2$$

where, in addition to the terms described for multi variable linear regression model, we included a term for interaction between  $x_1$  and  $x_2$  with a weight of  $\beta_4$ .

In addition, residuals were calculated as the difference between the predicted values and the observed values. We also performed F-statistics on the coefficients/weights to determine if they were significant.

**Distance analysis**—Experiments with 3 or more odors were used to analyze the effect of raphe modulation on the odor evoked population activity patterns in MCs and TCs. For every experiment, the integrated responses from the odor-only and odor-paired-with raphe activation trials were pooled together to calculate the covariance matrix. The first 3 principal components (accounting for  $\geq 90\%$  of the variance) were used to project the individual odor responses onto 3-dimensional space. The intra-odor distance in the PCA space was calculated as the mean pair-wise distance between the vectors belonging to the same odor under same conditions (odor only or odor paired with raphe activation) across different trials. In other words, we compared responses across multiple trials under equivalent conditions.

Pair wise distance was calculated as:

$$d_{intra}(o) = \sqrt{\sum_{i=1}^3 (x_i(o) - y_i(o))^2}$$

$o$  = odor identity

$x, y$  = projections of individual trials for same conditions in first 3 principal components

The inter odor distance was calculated as the mean pair wise distance between the vectors for different odors under the same condition (odor alone or odor plus raphe activation), normalized by the square root of products of intra-odor distances for the odors involved.

## Statistics

Non parametric statistical tests were used. No assumption of normality of data was made. Wilcoxon signed-rank test was used for repeated measurements of the same cell and also for the paired data sets. Wilcoxon rank-sum test was used for comparing all unpaired non-normal distributions. Between 2 to 13 animals per experiment were used. Effort was made to minimize the number of animals used and to obtain maximum amount of data per animal. The number of animals used and number of trials/repetitions done per animal were large enough to obtain a strong data set with statistical power, and is congruent with previously published studies. F statistics were used to evaluate the goodness of fit for regression analysis. Variance within a group was described as standard error of the mean (SEM).

No blinding was done and subjects were not randomized but the individual trials were randomized in a given experiment. Pseudorandom sequences were generated using Matlab and were used to control the identity of individual trials.

## Supplementary Material

Refer to Web version on PubMed Central for supplementary material.

## Acknowledgment

We thank the members of Murthy and Dulac labs for helpful discussions throughout the project, and David Gire, Jeremiah Cohen, and Monica Thanawala for comments on the manuscript. This work was supported by research grants from the NIH (VNM), a seed grant from the Harvard Brain Initiative (VNM) and fellowships from the NSF and the Mortimer and Theresa Sackler Foundation (ACP).

## References

1. Lee S-H, Dan Y. Neuromodulation of brain states. *Neuron*. 2012; 76:209–222. [PubMed: 23040816]
2. Marder E. Neuromodulation of neuronal circuits: back to the future. *Neuron*. 2012; 76:1–11. [PubMed: 23040802]
3. Cools R, Roberts AC, Robbins TW. Serotonergic regulation of emotional and behavioural control processes. *Trends Cogn. Sci.* 2008; 12:31–40. [PubMed: 18069045]
4. Dayan P, Huys QJM. Serotonin in affective control. *Annu. Rev. Neurosci.* 2009; 32:95–126. [PubMed: 19400722]
5. Liu Z, et al. Dorsal raphe neurons signal reward through 5-HT and glutamate. *Neuron*. 2014; 81:1360–1374. [PubMed: 24656254]
6. Dacks AM, Green DS, Root CM, Nighorn AJ, Wang JW. Serotonin modulates olfactory processing in the antennal lobe of *Drosophila*. *J. Neurogenet.* 2009; 23:366–377. [PubMed: 19863268]
7. Fonseca M, Murakami M, Mainen Z. Activation of dorsal raphe serotonergic neurons promotes waiting but is not reinforcing. *Curr. Biol.* 2015 doi:10.1016/j.cub.2014.12.002.
8. Hurley LM, Devilbiss DM, Waterhouse BD. A matter of focus: monoaminergic modulation of stimulus coding in mammalian sensory networks. *Curr Opin Neurobiol.* 2004; 14:488–95. [PubMed: 15321070]
9. Petzold GC, Hagiwara A, Murthy VN. Serotonergic modulation of odor input to the mammalian olfactory bulb. *Nat. Neurosci.* 2009; 12:784–791. [PubMed: 19430472]

10. Hilaire Gè. et al. The role of serotonin in respiratory function and dysfunction. *Respir. Physiol. Neurobiol.* 2010; 174:76–88. [PubMed: 20801236]
11. Jacobs BL, Azmitia EC. Structure and function of the brain serotonin system. *Physiol Rev.* 1992; 72:165–229. [PubMed: 1731370]
12. Ray RS, et al. Impaired respiratory and body temperature control upon acute serotonergic neuron inhibition. *Science.* 2011; 333:637–642. [PubMed: 21798952]
13. Hannon J, Hoyer D. Molecular biology of 5-HT receptors. *Behav. Brain Res.* 2008; 195:198–213. [PubMed: 18571247]
14. Cohen JY, Amoroso MW, Uchida N. Serotonergic neurons signal reward and punishment on multiple timescales. *eLife.* 2015; 4
15. Ranade SP, Mainen ZF. Transient firing of dorsal raphe neurons encodes diverse and specific sensory, motor, and reward events. *J. Neurophysiol.* 2009; 102:3026–3037. [PubMed: 19710375]
16. Dacks AM, Green DS, Root CM, Nighorn AJ, Wang JW. Serotonin modulates olfactory processing in the antennal lobe of *Drosophila*. *J. Neurogenet.* 2009; 23:366–377. [PubMed: 19863268]
17. Rhoades RW, Bennett-Clarke CA, Shi MY, Mooney RD. Effects of 5-HT on thalamocortical synaptic transmission in the developing rat. *J Neurophysiol.* 1994; 72:2438–50. [PubMed: 7884470]
18. Suzuki Y, Kiyokage E, Sohn J, Hioki H, Toida K. Structural basis for serotonergic regulation of neural circuits in the mouse olfactory bulb. *J. Comp. Neurol.* 2015; 523:262–280. [PubMed: 25234191]
19. Varga V, et al. Fast Synaptic Subcortical Control of Hippocampal Circuits. *Science.* 2009; 326:449–453. [PubMed: 19833972]
20. Nagayama S, Homma R, Imamura F. Neuronal organization of olfactory bulb circuits. *Front. Neural Circuits.* 2014; 8:98. [PubMed: 25232305]
21. Haberly LB. Parallel-distributed processing in olfactory cortex: new insights from morphological and physiological analysis of neuronal circuitry. *Chem Senses.* 2001; 26:551–76. [PubMed: 11418502]
22. Fukunaga I, Berning M, Kollo M, Schmaltz A, Schaefer A. Two distinct channels of olfactory bulb output. *Neuron.* 2012; 75:320–329. [PubMed: 22841316]
23. Giessel AJ, Datta SR. Olfactory maps, circuits and computations. *Curr. Opin. Neurobiol.* 2014; 24:120–132. [PubMed: 24492088]
24. McLean JH, Shipley MT. Serotonergic afferents to the rat olfactory bulb: I. Origins and laminar specificity of serotonergic inputs in the adult rat. *J. Neurosci.* 1987; 7:3016–3028. [PubMed: 2822862]
25. Steinfeld R, Herb JT, Sprengel R, Schaefer AT, Fukunaga I. Divergent innervation of the olfactory bulb by distinct raphe nuclei. *J. Comp. Neurol.* 2015; 523:805–813. [PubMed: 25420775]
26. Liu S, Aungst JL, Puche AC, Shipley MT. Serotonin modulates the population activity profile of olfactory bulb external tufted cells. *J. Neurophysiol.* 2012; 107:473–483. [PubMed: 22013233]
27. Hardy A, Palouzier-Paulignan B, Duchamp A, Royet J-P, Duchamp-Viret P. 5-hydroxytryptamine action in the rat olfactory bulb: In vitro electrophysiological patch-clamp recordings of juxtglomerular and mitral cells. *Neuroscience.* 2005; 131:717–731. [PubMed: 15730876]
28. Nakamura K, Matsumoto M, Hikosaka O. Reward-dependent modulation of neuronal activity in the primate dorsal raphe nucleus. *J Neurosci.* 2008; 28:5331–43. [PubMed: 18480289]
29. Chen T-W, et al. Ultrasensitive fluorescent proteins for imaging neuronal activity. *Nature.* 2013; 499:295–300. [PubMed: 23868258]
30. Haddad R, et al. Olfactory cortical neurons read out a relative time code in the olfactory bulb. *Nat. Neurosci.* 2013; 16:949–957. [PubMed: 23685720]
31. Ray RS, et al. Impaired respiratory and body temperature control upon acute serotonergic neuron inhibition. *Science.* 2011; 333:637–642. [PubMed: 21798952]
32. Wachowiak M. All in a sniff: olfaction as a model for active sensing. *Neuron.* 2011; 71:962–973. [PubMed: 21943596]
33. Adam Y, et al. Functional transformations of odor inputs in the mouse olfactory bulb. *Front. Neural Circuits.* 2014; 8:129. [PubMed: 25408637]

34. Kikuta S, Fletcher M, Homma R, Yamasoba T, Nagayama S. Odorant response properties of individual neurons in an olfactory glomerular module. *Neuron*. 2013; 77:1122–1135. [PubMed: 23522047]
35. Zhao S, et al. Cell-type Specific Optogenetic mice for dissecting neural circuitry function. *Nat. Methods*. 2011; 8:745–752. [PubMed: 21985008]
36. Kapoor V, Urban NN. Glomerulus-specific, long-latency activity in the olfactory bulb granule cell network. *J. Neurosci*. 2006; 26:11709–11719. [PubMed: 17093092]
37. Gire DH, et al. Mitral cells in the olfactory bulb are mainly excited through a multistep signaling path. *J. Neurosci. Off. J. Soc. Neurosci*. 2012; 32:2964–2975.
38. Najac M, De Saint Jan D, Reguero L, Grandes P, Charpak S. Monosynaptic and polysynaptic feed-forward inputs to mitral cells from olfactory sensory neurons. *J. Neurosci. Off. J. Soc. Neurosci*. 2011; 31:8722–8729.
39. Friedrich RW, Wiechert MT. Neuronal circuits and computations: pattern decorrelation in the olfactory bulb. *FEBS Lett*. 2014; 588:2504–2513. [PubMed: 24911205]
40. Miyazaki K, et al. Optogenetic activation of dorsal raphe serotonin neurons enhances patience for future rewards. *Curr. Biol*. 2014; 24:2033–2040. [PubMed: 25155504]
41. Gracia-Llanes FJ, et al. Synaptic connectivity of serotonergic axons in the olfactory glomeruli of the rat olfactory bulb. *Neuroscience*. 2010; 169:770–780. [PubMed: 20493930]
42. Commons KG. Locally collateralizing glutamate neurons in the dorsal raphe nucleus responsive to substance P contain vesicular glutamate transporter 3 (VGLUT3). *J. Chem. Neuroanat*. 2009; 38:273–281. [PubMed: 19467322]
43. Fremeau RT Jr, Voglmaier S, Seal RP, Edwards RH. VGLUTs define subsets of excitatory neurons and suggest novel roles for glutamate. *Trends Neurosci*. 2004; 27:98–103. [PubMed: 15102489]
44. Qi J, et al. A glutamatergic reward input from the dorsal raphe to ventral tegmental area dopamine neurons. *Nat. Commun*. 2014; 5
45. Otazu GH, Chae H, Davis MB, Albeanu DF. Cortical feedback decorrelates olfactory bulb output in awake mice. *Neuron*. 2015; 86:1461–1477. [PubMed: 26051422]
46. Burton SD, Urban NN. Greater excitability and firing irregularity of tufted cells underlies distinct afferent-evoked activity of olfactory bulb mitral and tufted cells. *J. Physiol*. 2014; 592:2097–2118. [PubMed: 24614745]
47. Scott JW. Electrophysiological identification of mitral and tufted cells and distributions of their axons in olfactory system of the rat. *J Neurophysiol*. 1981; 46:918–31. [PubMed: 6271931]
48. Kiselycznyk CL, Zhang S, Linstner C. Role of centrifugal projections to the olfactory bulb in olfactory processing. *Learn Mem*. 2006; 13:575–9. [PubMed: 16980549]
49. Rothermel M, Carey RM, Puche A, Shipley MT, Wachowiak M. Cholinergic inputs from basal forebrain add an excitatory bias to odor coding in the olfactory bulb. *J. Neurosci. Off. J. Soc. Neurosci*. 2014; 34:4654–4664.
50. Shea SD, Katz LC, Mooney R. Noradrenergic induction of odor-specific neural habituation and olfactory memories. *J. Neurosci*. 2008; 28:10711–10719. [PubMed: 18923046]
51. Atasoy D, Aponte Y, Su HH, Sternson SM. A FLEX switch targets Channelrhodopsin-2 to multiple cell types for imaging and long-range circuit mapping. *J Neurosci*. 2008; 28:7025–30. [PubMed: 18614669]
52. Soucy ER, Albeanu DF, Fantana AL, Murthy VN, Meister M. Precision and diversity in an odor map on the olfactory bulb. *Nat. Neurosci*. 2009; 12:210–220. [PubMed: 19151709]
53. Markopoulos F, Rokni D, Gire DH, Murthy VN. Functional properties of cortical feedback projections to the olfactory bulb. *Neuron*. 2012; 76:1175–1188. [PubMed: 23259952]

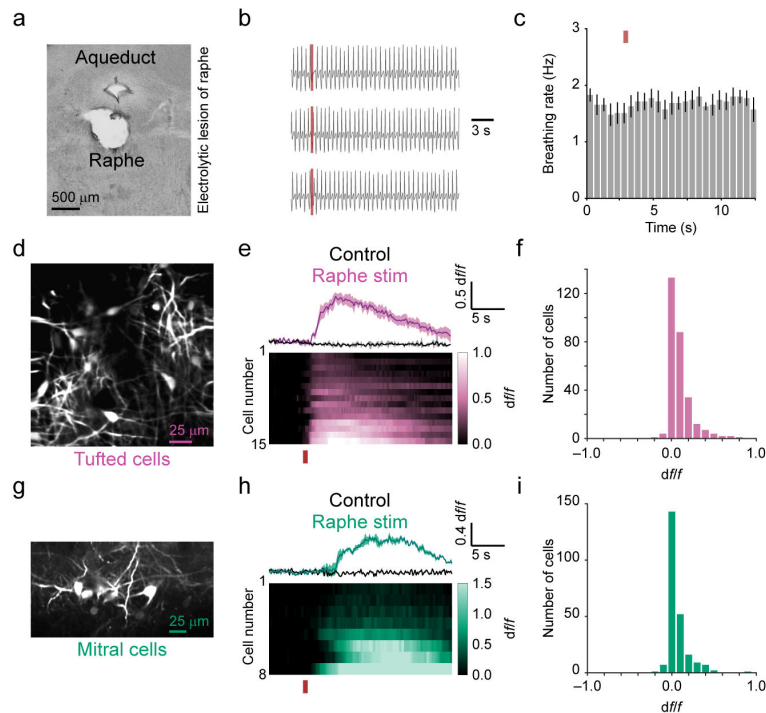


**Figure 1. Raphe stimulation excites mitral and tufted cells at rest**

- a) Histological section showing an electrolytic lesion in the raphe nucleus introduced with the stimulating electrode at the end of an experiment.
- b) Three exemplar trials showing breathing traces measured with a chest strap around the time of raphe stimulation (three 1ms pulses at 10Hz; orange vertical bars). Upward deflections correspond to inhalation.
- c) Peristimulus time histogram (PSTH) of breathing rate across 5 animals. Orange bar denotes time of raphe stimulation and black lines are SEM.
- d) Resting fluorescence image of TCs in an exemplar experiment shown in (e).
- e) Average trace showing TC response to raphe activation (purple). Time course of fractional fluorescence intensity for all cells in the field of view in (d) in response to raphe activation (orange bars). Cell 15 is plotted at top.
- f) Bar plot of all imaged TCs showing fluorescence change in trials with raphe stimulation when compared to blank trials with no raphe stimulation (288 cells, 12 mice,  $p = 9.80 \times 10^{-29}$ , Wilcoxon signed-rank).
- g) Resting fluorescence image of MCs in one experiment, analyzed in (h),(i).
- h) Average trace showing an example MC responding to activation of raphe (bluish-green). Time course of fractional fluorescence intensity for all cells in the field of view in (g) in response to raphe activation (orange bar). Cell 7 is plotted at top.
- i) Bar plot of fluorescence changes in all imaged MCs for trials with raphe stimulation compared to blank trials with no stimulation (238 cells, 13 mice,  $p = 4.68 \times 10^{-10}$ , Wilcoxon signed-rank).



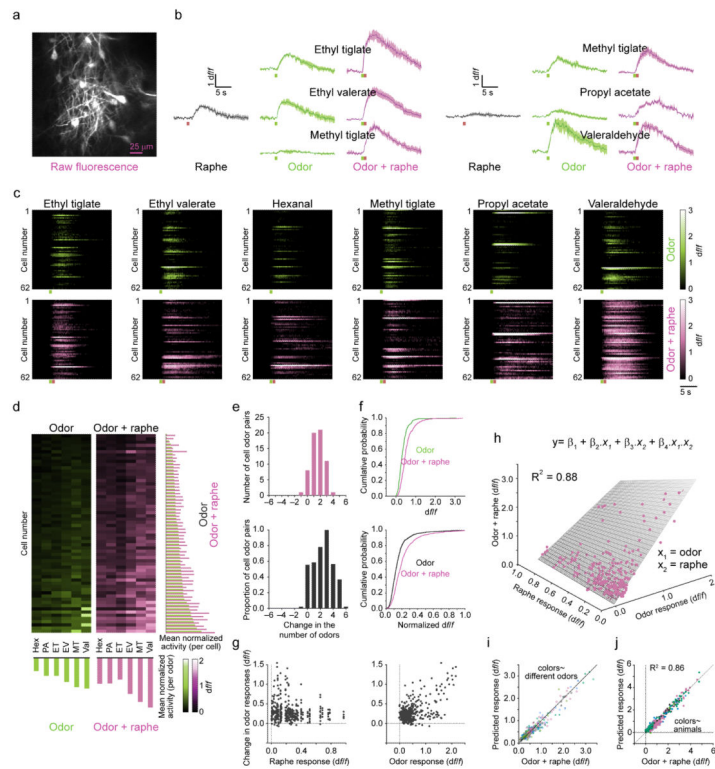


**Figure 2. TC odor responses are sensitized by raphe inputs**

- a) 2-photon image showing resting fluorescence of GCaMP6s in TCs.
- b) Time course of fluorescence responses of two TCs to raphe stimulation (black), odor stimulation (light green) and raphe and odor stimulation (purple). Bars denote odor timing (light green) and raphe stimulation timing (orange). Error bars are SEM.
- c) Time course of responses to 6 odors in 62 TCs in the imaged region shown in (a). Light green and orange bars at bottom indicate the timing of the odor and raphe stimulation, respectively.
- d) Heat map representing the double rank ordered odor responses without (light green) and with (purple) raphe activation. Each row indicates the odor response amplitudes of single cells, with the rows themselves rank ordered in increasing amplitude of responses (summed across all odors). The order of cells was determined in the left panel and was maintained for the right panel (with raphe stimulation) for direct comparison. Bar plots on the right show the normalized summed activity of single cells and bar plots at the bottom show normalized summed activity for odors.
- e) Bar plot (top) showing the change in the number of odors that elicited responses without and with raphe stimulation for cells shown in c (372 cell-odor pairs,  $p = 7.50 \times 10^{-13}$ , Wilcoxon signed-rank). Bar plot (bottom) showing the change in the number of odors that elicited responses without and with raphe stimulation for all cell odor pairs from 6 animals (1087 cell-odor pairs,  $p = 1.68 \times 10^{-10}$ , Wilcoxon signed-rank).
- f) Cumulative distribution of the change in fluorescence for TCs without raphe stimulation (light green) or with raphe stimulation (purple) for all the cell odor pairs shown in c and d (top). Same for TCs without (black) or with raphe stimulation (purple) for all the cell odor pairs ( $n=1087$ ) across 6 animals (bottom).

- g) Scatter plots showing change in odor response for each TC when the raphe is stimulated (compared to odor response on its own), as a function of raphe response (left) and odor response (right) for that TC. Each dot is a single cell odor pair.
- h) Three dimensional scatter plot showing the responses for TCs (372 odor cell pairs) for odor and raphe stimulation. The prediction surface, shown as a grid, is from the interaction based regression model (see Methods).
- i) Scatter plot showing the predicted based on interactive model vs observed responses for odor and raphe stimulation (colors depict different odors,  $R^2 = 0.88$ ).
- j) Scatter plot showing the predicted vs observed responses for odor and raphe stimulation (colors depict different animals,  $R^2 = 0.86$  for  $n=6$  animals, 1087 cell-odor pairs,  $p = 1.29 \times 10^{-21}$ , F test).

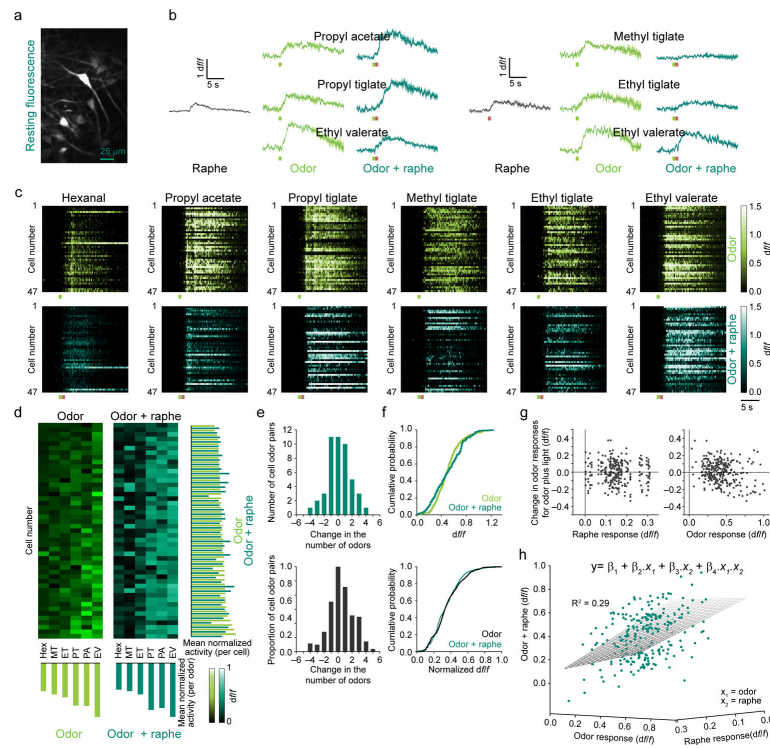


**Figure 3. MC odor responses are bidirectionally modulated by raphe inputs**

- a) 2-photon image showing resting fluorescence of GCaMP6s in MCs.
- b) Time courses of fluorescence of two MCs in response to raphe stimulation (black), odor stimulation (light green) and raphe and odor stimulation (bluish-green). Bars are odor timing (light green) and raphe stimulation timing (orange). Error bars are SEM.
- c) Time course of responses to 6 odors in 47 MCs in the imaged region. Green and red bars at bottom indicate the timing of the odor and raphe stimulation, respectively.
- d) Heat map representing the double rank ordered odor responses without (light green) and with (bluish-green) raphe activation. Each row indicates the odor response amplitudes of single cells, with the rows themselves rank ordered in increasing amplitude of responses (summed across all odors). The order of cells was determined in the left panel and was maintained for the right panel (with raphe stimulation) for direct comparison. Bar plots on the right show the normalized summed activity of single cells and bar plots at the bottom show normalized summed activity for odors.
- e) Bar plot (top) showing the change in the number of odors that elicited responses without and with raphe stimulation for cells shown in c ( $p = 0.61$  for  $n=47$  cells for Wilcoxon signed-rank). (Bottom) Bar plot showing the change in the number of odors that elicited responses without and with raphe stimulation for all cell odor pairs ( $p = 0.85$  for 1050 cells from 7 animals, Wilcoxon signed-rank).
- f) Cumulative distribution of the change in fluorescence for MCs without (light green) or with (bluish-green) raphe stimulation for all the cell odor pairs shown in c and d (top). Cumulative distribution of the change in fluorescence for MCs without raphe stimulation (black) or with raphe stimulation (bluish-green) for all the cell-odor pairs ( $n=1050$ ) across 7 animals (bottom).

- g) Scatter plots showing change in odor response for each MC when the raphe is stimulated (compared to odor response on its own), as a function of raphe response (left) and odor response (right) for that MC. Each dot is a single cell odor pair.
- h) Three dimensional scatter plot showing the responses for MCs (282 odor cell pairs) for odor and raphe stimulation ( $R^2 = 0.29$ ). Grid shows the prediction manifold based on interaction based regression model (see methods).

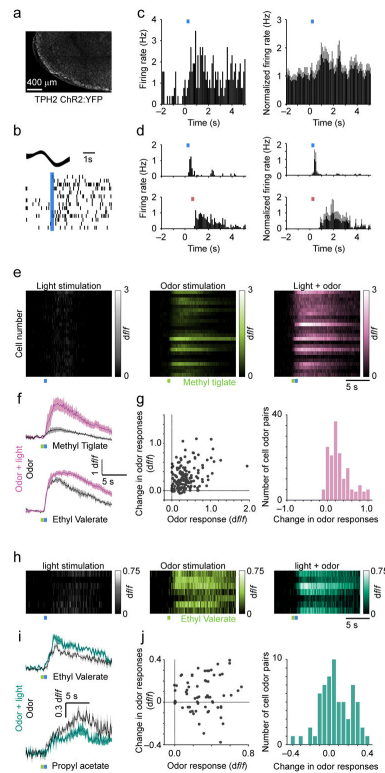


**Figure 4. Optogenetic activation of raphe leads to excitation of principal cells**

- a) Confocal image of the raphe fibers innervating different layers of the OB in a TPH2-ChR2:YFP mouse.
- b) Extracellular spikes from an isolated unit (820 spikes superimposed at top) recorded in the OB are represented in a raster plot (bottom). Twenty trials of dorsal surface stimulation with blue light (timing indicated by blue bar).
- c) PSTH of activity of a single putative M/TC (left) in the TPH2-ChR2:YFP mouse exhibiting excitation from rest when raphe fibers are activated via blue light (100 ms bins, same for all PSTHs). Population PSTH of all putative M/TCs (right) from extracellular recordings in the TPH2-ChR2:YFP mouse (n=17 cells). Gray shading indicates SEM.
- d) PSTH of activity in a single putative M/TC in the TPH2-ChR2:YFP mouse reveals excitatory responses to blue light stimulation (top left, timing indicated by the blue bar) and electrical stimulation of the raphe (bottom left, timing indicated by orange bar). Population PSTH of all putative M/TCs both with electrical stimulation (bottom right) and ChR2 stimulation (top right) in the TPH2-ChR2:YFP mouse (n=9 cells). Firing rate in the resting period for each cell was normalized before averaging, and the final average was normalized to the peak for clarity of display.
- e) Time course of responses in 24 TCs in 3 animals for i) light stimulation (gray), ii) odor stimulation (light green, methyl tiglate) and iii) odor plus light stimulation (purple). Light green and blue bars at bottom indicate the timing of the odor and ChR2 stimulation, respectively.
- f) Time courses of fluorescence changes in a single TC in response to odor stimulation alone (black) and odor stimulation along with light stimulation of raphe (purple) for 2 different odors. Shading indicates SEM.

g) Scatter plot showing change in odor responses caused by concurrent raphe stimulation, as a function of odor response (left). Bar graph (right) showing distribution of changes in odor responses in TCs caused by optical stimulation of the raphe for 144 odor-cell pairs from 3 animals ( $p = 1.2 \times 10^{-23}$  for Wilcoxon signed-rank test).

h) Time course of responses in 7 MCs from 2 animals for i) light stimulation (gray), ii) odor stimulation (light green, ethyl valerate) and iii) odor plus light stimulation (bluish-green). Light green and blue bars at bottom indicate the timing of the odor and ChR2 stimulation, respectively.

i) Time courses of fluorescence changes in a single MC in response to odor stimulation alone (black) and odor stimulation along with light stimulation of raphe (bluish-green) for 2 different odors. Shading indicates SEM.

j) Scatter plot showing change in odor responses in MCs caused by concurrent raphe stimulation, as a function of odor response (left). Bar graph showing distribution of changes in odor responses in MCs caused by optical stimulation of the raphe for 64 odor-cell pairs from 2 animals (right).



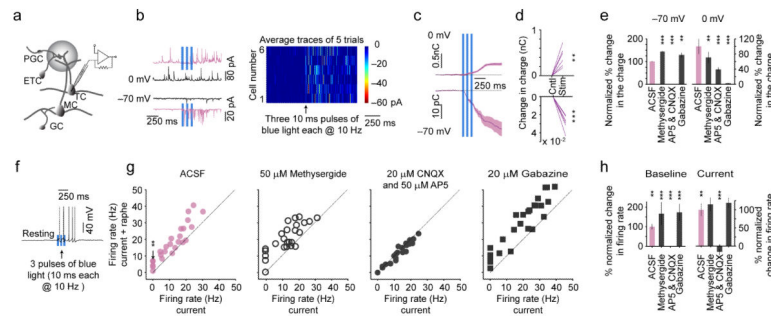


**Figure 5. Modulation of TCs by optogenetic activation of raphe projections in main olfactory bulb slices**

- a) Schematic diagram depicting TC recordings from OB slices.
- b) (Left) Whole cell voltage clamp recordings from a TC at 0mV and  $-70$  mV showing IPSCs (top) and EPSCs (bottom) with (purple) and without (black) raphe fiber activation. (Right) Average time series for 6 TCs showing EPSCs elicited by brief optogenetic activation of raphe fibers (black arrow).
- c) (Bottom) Integrated charge transfer in a TC at  $-70$  mV with (purple) optogenetic activation of raphe fibers. Blue bars depict the timing of raphe fiber activation. (Top) change in integrated charge transfer at 0 mV with (purple) optogenetic activation of raphe fibers (Black dotted reference line).
- d) Summary of all 6 recorded TCs, showing increase in both inhibitory charge transfer (top,  $p = 3.1 \times 10^{-27}$  for 6 cells from 4 animals, Wilcoxon signed-rank test) and excitatory charge transfer (bottom,  $p = 3.3 \times 10^{-3}$  for Wilcoxon signed-rank test,  $n = 6$  cells from 4 animals) by light stimulation.
- e) Normalized percentage change in the charge transfer for EPSCs (left,  $-70$ mV) and IPSCs (right, 0mV) in presence of different antagonists: 5-HT receptor antagonist ( $50 \mu\text{M}$  methysergide,  $p = 5.01 \times 10^{-4}$  and  $p = 3.92 \times 10^{-3}$  for excitatory and inhibitory charge transfer respectively, Wilcoxon rank-sum test,  $n = 8$  cells from 5 animals), glutamate receptor antagonists ( $20 \mu\text{M}$  CNQX and  $50 \mu\text{M}$  AP5,  $p = 7.61 \times 10^{-29}$  and  $2.10 \times 10^{-7}$  for excitatory and inhibitory charge transfer respectively, Wilcoxon rank-sum test,  $n = 7$  cells from 5 animals), and GABA receptor antagonist ( $20 \mu\text{M}$  gabazine,  $p = 2.0 \times 10^{-3}$  and  $p = 1.92 \times 10^{-21}$  for excitatory and inhibitory charge transfer respectively, Wilcoxon rank-sum test,  $n = 6$  cells from 6 animals). Data for some conditions are not visible since they are close to 0 and significance is shown with \*. \* signifies  $p < 0.05$ , \*\* signifies  $p < 0.01$  and \*\*\* signifies  $p < 0.001$ .
- f) Example trace of a TC recorded under current clamp showing spikes in response to raphe fibers activation. Blue bars indicate blue light timing.
- g) Scatter plots comparing the firing rate of TCs for different step current injection with and without serotonergic fiber activation in presence of different antagonists: no drug (purple,  $p = 1.21 \times 10^{-3}$ , Wilcoxon rank-sum test,  $n = 5$  cells from 5 animals), glutamate receptor antagonists ( $20 \mu\text{M}$  CNQX and  $50 \mu\text{M}$  AP5, black solid circles,  $p = 1.43 \times 10^{-8}$ , Wilcoxon rank-sum test,  $n = 5$  cells from 5 animals), 5-HT receptor antagonist ( $50 \mu\text{M}$  methysergide, open circles,  $p = 0.072$ ,  $n = 5$  cells from 3 animals, Wilcoxon rank-sum test), and GABA receptor antagonist ( $20 \mu\text{M}$  gabazine, squares,  $p = 0.068$ ,  $n = 5$  cells from 4 animals, Wilcoxon

rank-sum test). Firing rates calculated for an 800 ms period starting at the time of first light stimulation. \*\* signifies  $p < 0.01$ .

h) Light-triggered changes in firing rates of TCs for no current injection (left,  $p = 9.21 \times 10^{-3}$ , Wilcoxon rank-sum test,  $n = 5$  cells from 4 animals) and averaged across different levels of current injections (right). The changes for different pharmacological manipulations were normalized to the condition with no drugs applied (ACSF). \* signifies  $p < 0.05$ , \*\* signifies  $p < 0.01$  and \*\*\* signifies  $p < 0.001$ .

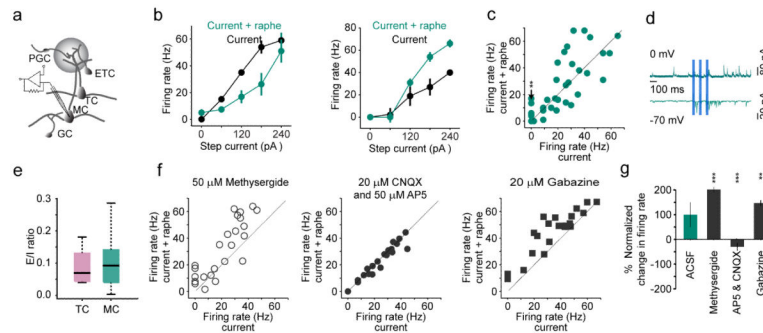


**Figure 6. Modulation of MC activity by optogenetic activation of raphe fibers**

- a) Schematic diagram depicting MC recordings from OB slices.
- b) Plot of the relationship between injected current and firing rate for 2 different MCs showing both inhibitory and excitatory effects of raphe fiber activation.
- c) Scatter plots comparing the firing rate of MCs for different step current injection with and without raphe fiber activation. Arrow points to trials where light stimulation induced firing in MCs that were quiescent ( $p = 2.0 \times 10^{-3}$ , Wilcoxon rank-sum test,  $n = 7$  cells from 4 animals). \*\* signifies  $p < 0.01$ .
- d) Whole cell voltage clamp recordings from a MC at 0mV and  $-70$  mV showing IPSCs (top) and EPSCs (bottom) with raphe fiber activation. Blue bars depict the timing of ChR2 fiber stimulation.
- e) Ratio of integrated excitatory to inhibitory charge transfer in TCs and MCs ( $n = 6$  each) following optogenetic stimulation of raphe fibers.
- f) Scatter plots comparing the firing rate of MCs for different step current injection with and without raphe fiber activation in presence of different antagonists: 5-HT receptor antagonist ( $50 \mu\text{M}$  methysergide, open circles,  $p = 1.1 \times 10^{-19}$ , Wilcoxon rank-sum test,  $n = 5$  cells from 3 animals), glutamate receptor antagonists ( $20 \mu\text{M}$  CNQX and  $50 \mu\text{M}$  AP5, solid circles,  $p = 7.2 \times 10^{-31}$ , Wilcoxon rank-sum test,  $n = 5$  cells from 4 animals), and GABA antagonist ( $20 \mu\text{M}$  gabazine, squares,  $p = 8.79 \times 10^{-3}$ , Wilcoxon rank-sum test,  $n = 5$  cells from 4 animals).
- g) Average light-triggered changes in firing rates of all MCs averaged across different levels of current injections. The changes for different pharmacological manipulations were normalized to the condition with no drugs applied. \* signifies  $p < 0.05$ , \*\* signifies  $p < 0.01$  and \*\*\* signifies  $p < 0.001$ .

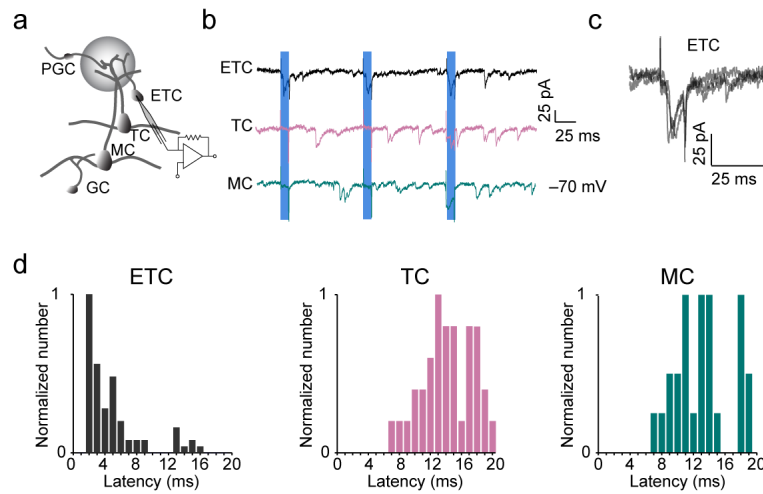


**Figure 7. ETCs receive direct excitatory inputs from raphe fibers**

a) Schematic diagram depicting ETC recordings from OB slices.

b) Whole cell voltage clamp recordings from at  $-70$  mV showing short latency EPSCs in ETC (top) and long latencies in TC (middle) and MC (bottom). Timing of light stimulus is shown in blue. –

c) Four successive trials from an ETC, showing short latency EPSCs at  $-70$  mV for raphe fiber activation.

d) Histograms showing the latencies of EPSCs in ETCs (gray,  $n=10$  cells), TCs (purple,  $n=8$ ) and MCs (bluish-green,  $n=6$ ) in response to optogenetic activation of raphe fibers ( $p=3.2 \times 10^{-17}$  and  $p=2.4 \times 10^{-20}$  for TC and MC respectively, Wilcoxon rank-sum test).

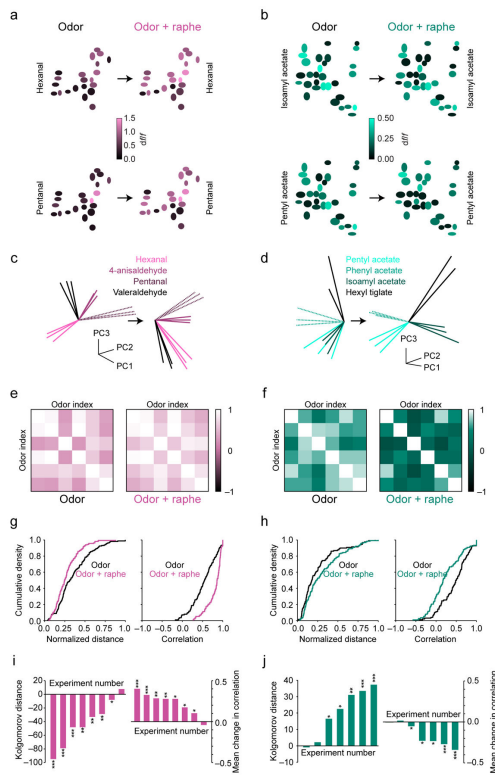


**Figure 8. Raphe activation leads to sensitization of TC odor responses and decorrelation of MC odor responses**

- a) Pseudo-color plot showing the pattern of odor responses in a region of interest for in vivo experiment with TCs for two odors without (left) and with (right) raphe activation. Ellipses denote individual cell bodies.
- b) Similar plot for MC population from a different experiment.
- c) Principal component projections of TC responses from one experiment in the space of the first 3 components, for 4 different odors without and with raphe activation.
- d) Principal component projections for MC responses in a different experiment.
- e) Matrix showing the correlation between odor responses of TCs (6 odors) without (left) and with (right) raphe stimulation ( $p = 2.16 \times 10^{-7}$  for Wilcoxon rank-sum test,  $n = 6$  odors). Note that diagonal elements have a value of 1 by definition.
- f) Analogous matrix for MCs ( $p = 7.8 \times 10^{-4}$  for Wilcoxon rank-sum test,  $n = 6$  odors).
- g) Cumulative density plots comparing the inter-odor distances measured in PCA space (left) and through direct correlation between different odors (right) for the TC experiment shown in panels a and c.
- h) Analogous density plots for MC experiment illustrated in b and d.
- i) Bar graphs depicting change in the inter-odor separation for TC population when raphe is stimulated for 8 separate experiments ( $p < 0.05$ , Wilcoxon rank sum test,  $n = 8$  animals, see Methods for the criterion). The change was calculated as the Kolmogorov distance between the cumulative density plots in PCA space (left) and as change in the correlation (right).

j) Bar graphs depicting change in the inter-odor separation for MC population when raphe is stimulated for 7 separate experiments ( $p < 0.05$ , Wilcoxon rank sum test,  $n=7$  animals, see Methods for details).

Author Manuscript

Author Manuscript

Author Manuscript

Author Manuscript